Received: 31 May 2018 | Revised: 19 July 2018 | Accepted: 19 July 2018

DOI: 10.1002/sia.6522

SPECIAL ISSUE ARTICLE

WILEY SURFACE and INTERFACE ANALYSIS

Argon cluster cleaning of Ga^+ FIB-milled sections of organic and hybrid materials*

Mariavitalia Tiddia[1,2] | Martin P. Seah[2] | Alex G. Shard[2] | Guido Mula[1] | Rasmus Havelund[2] | Ian S. Gilmore[2]

[1] Dipartimento di Fisica, Università degli Studi di Cagliari, S. P. 8 Km 0.700, 09042 Monserrato, Italy

[2] National Physical Laboratory, Hampton Road, Teddington TW11 0LW, UK

Correspondence
M. P. Seah, National Physical Laboratory, Hampton Road, Teddington TW11 0LW, UK.
Email: martin.seah@npl.co.uk

Funding information
European Union; UK Department for Business, Energy & Industrial Strategy

Secondary ion mass spectrometry studies have been made of the removal of the degraded layer formed on polymeric materials when cleaning focused ion beam (FIB)-sectioned samples comprising both organic and inorganic materials with a 30-keV Ga^+ FIB. The degraded layer requires a higher-than-expected Ar gas cluster ion beam (GCIB) dose for its removal, and it is shown that this arises from a significant reduction in the layer sputtering yield compared with that for the undamaged polymer. Stopping and Range of Ions in Matter calculations for many FIB angles of incidence on flat polymer surfaces show the depth of the damage and of the implantation of the Ga^+ ions, and these are compared with the measured depth profiles for Ga^+-implanted flat polymer surfaces at several angles of incidence using an Ar^+ GCIB. The Stopping and Range of Ions in Matter depth and the measured dose give the sputtering yield volume for this damaged and Ga^+-implanted layer. These, and literature yield values for Ga^+ damaged layers, are combined on a plot showing how the changing sputtering yield is related to the implanted Ga density for several polymer materials. This plot contains data from both the model flat poly(styrene) surfaces and FIB-milled sections showing that these 2 surfaces have the same yield reduction. The results show that the damaged and Ga^+-implanted layer's sputtering rate, after FIB sectioning, is 50 to 100 times lower than for undamaged polymers and that it is this reduction in sputtering rate, rather than any development of microtopography, that causes the high Ar^+ GCIB dose required for cleaning these organic surfaces.

KEYWORDS

depth profiling, FIB, organics, polymers, SIMS

1 | INTRODUCTION

Secondary ion mass spectrometry (SIMS) has been used for many years with focused ion bombardment (FIB) to provide analysis through very local sections of materials to depths of many micrometres.[1-7] This complements, very nicely, the traditional sputter depth profiling of uniform layers where the total depths are generally smaller but where depth resolutions may be superior and may be typically around 1% of the depth sputtered.[8,9] The FIB sections are generally made using a focused Ga^+ ion beam because, practically, such beams are available with the smallest spot sizes,[4] with reasonable beam currents and sputtering rates. During the milling, Ga^+ ions both remove material and are implanted in the surface of the remaining material to be analyzed by the SIMS. Excellent examples of the method for inorganic samples have been shown by Whitby et al,[6] Schneider et al,[7] and many others.

In the study of organic layers, SIMS has been used for a very long time to analyze the outermost surface,[10,11] but damage effects, due to the primary ions,[12-14] have been observed in depth profiles. Similar damage effects caused by the X-rays used in X-ray photoelectron spectroscopy have also been observed.[15] However, a recent major

*Dedicated to the memory of David Briggs, founding editor of Surface and Interface Analysis and a scientist of immense talent and vision.

advance has been made by the introduction and development of argon gas cluster ion beams (GCIBs) for depth profiling[16-18] where the material is removed leaving a very clean organic surface with minimal degradation. Until that development, SIMS depth profiling of organic materials was not routine. Ar^+ GCIBs work very well indeed and have led to excellent depth profiles for organic systems involving both thick and delta layers.[19,20] What is not so easy is the case of structures in which both organic and inorganic materials are present. The inorganic materials sputter at only 1% of the rate of organic materials for argon clusters when the energy per argon atom is greater than 10 eV. This small relative rate decreases even further, falling to less than 0.1%, with energies per atom below 1 eV.[21] Thus, direct depth profiling of these structures using Ar^+ GCIBs is difficult and liable to poor depth resolution even if the inorganic layers are thin. Structures with uneven overlayers but smooth interfaces, like membrane electrode assemblies used in fuel and other cells,[22] become impossible by the direct approach but are more easily tackled by FIB-sectioning.

To overcome this problem, we have studied Ga^+ FIB sectioning of samples involving both inorganic and organic materials.[22] The sample for this study is made using a glass multichannel plate (MCP) electron multiplier with 10-μm diameter tube diameters[18] which are filled with either poly(styrene) (PS) or poly(methyl methacrylate) (PMMA). This composite sample sections very nicely,[22] but, of course, the final surface has been heavily exposed to the Ga^+ milling ions. The surface layer of the polymers is highly damaged and implanted with Ga^+. Using the Ar^+ GCIB to remove this layer requires quite a high dose,[22] which may be caused by needle cones similar to the microtopography that can be observed in the crater base of FIB-milled sections of some inorganic materials. If so, the development of such microtopography would require study to minimize it. Alternatively, the high dose may be caused by something inherent in the FIB process. The present work seeks to clarify these issues. Through a better understanding of the requirement for cleaning, the process may be made more efficient or controlled.

In our previous study,[22] it was shown that the angular dependence of the sputtering yield of the polymer by the Ga^+ ion beam, combined with the focused spot size, the raster array pitch, and the sputtering dose, would lead to the final section wall surface being not parallel to the Ga^+ ion beam direction but at some 5 to 10° inclined to that direction. This was confirmed by atomic force microscope measurements. The final surface is thus both removed by, and implanted by, Ga^+ ions at some 80 to 85° incidence. The present study therefore analyses, inter alia, the cleaning, by an Ar^+ GCIB, of the surface of PS implanted by Ga^+ ions at various doses and incident angles to the surface normal.

2 | EXPERIMENTAL

In this study, 2 categories of sample were prepared: one to study implantation effects on flat surfaces and one to study the behavior in FIB-milled sectioning. The first category was high purity Goodfellow PS sheets, 1.2 mm thick, used to study the effect of the Ga^+ ion angle of incidence and dose. The second category of sample comprised hybrid inorganic and organic structures suitable as archetypes for analysis. As discussed elsewhere,[22] these were made by pressing either PS or PMMA into the MCP surface and then annealing it at 210°C under load in a vacuum oven for 5 hours. The MCP is made from sintered glass tubes, with a hole diameter of 10 μm, in a hexagonal array tilted at ~10° to the MCP surface normal. The hot pressing fills these tubes with polymer. The inner surfaces of the tubes have a surface coating to enhance the electron multiplication required for its original application. Studies were also made of unfilled MCPs. The glass of the MCP occupies 37% of the volume with the remainder either unfilled (vacuum) or filled with polymer.

The SIMS studies are made in IoN-TOF SIMS 5 which has a dual Ga^+ FIB and Ar^+ GCIB sputter profiling ion source mounted at 45° to the sample surface. The Ga^+ FIB source is operated at 30-keV beam energy, and the Ar^+ GCIB uses 10-keV Ar^+ clusters with a mean size of 2500 atoms. The implantation on flat surfaces uses the Ga^+ beam rastering an area 200 μm × 200 μm with 256 × 256 pixels at a beam current of 20 nA and a dwell time of 2 to 50 μs/pixel. The FIB sections use the Ga^+ beam rastering 120 μm × 80 μm, and sections are generated using 1 to 3 milling passes per scan. After FIB-milling a section using the Ga^+ beam, the sample is rotated 180° about its surface normal for Ar^+ GCIB cleaning over an area 500 μm × 500 μm. Secondary ion mass spectrometry analysis uses a 30-keV Bi_3^+ ion beam, also at 45° to the sample surface but in an azimuth at 90° to the Ga^+ and Ar^+ GCIB beam azimuths. Image areas for reconstructing the depth profiles are 200 μm × 200 μm with profiles mostly from an area 80 μm × 20 μm.

A few samples were studied for Ga^+ implantation at angles other than 45°. For these, the samples were mounted on a small wedge to tilt them. At the edge of the sample, a small grid allowed the Ga^+ raster scan setting to be adjusted to be the same area on the sample for each angle. After implantation, the samples were tilted to the horizontal and conventional depth profiles were made. Measurements of the depth sputtered by the Ga^+ ions were made for implants of 80 and 160 Ga^+ ions/nm^2, by AFM, across a knife edge shadow.

A schematic of the glass-polymer hybrid sample with a FIB-milled surface is shown in Figure 1A. To reduce damage and redeposition on the final section, FIB milling is made with a raster that starts at the lower left in Figure 1A and finishes at the top right with the final sectional surface to be studied. Section surfaces are made with 1 to 3 passes of the full raster to extend the depth of the cut but, in the present context, we see no differences between these final surfaces except the depth over which they extend.[22]

3 | THEORY

The geometry of an FIB-milled section is shown in Figure 1A, where the Ga^+ beam enters from the top right. All of the FIB-milled sections discussed in this work relate to these hybrid glass-polymer samples. An imaginary slice through the FIB-milled surface is shown in Figure 1 B rotated clockwise through 45° so that the Ga^+ beam is now vertical. The implanted Ga^+ ions may be deposited to a certain depth, which may be calculated using the Stopping and Range of Ions in Matter (SRIM) program.[23] Used directly, SRIM allows the implantation of many ions, but each new ion is into the same pure undamaged sample. In the continuum process of milling the section, this deposition will have

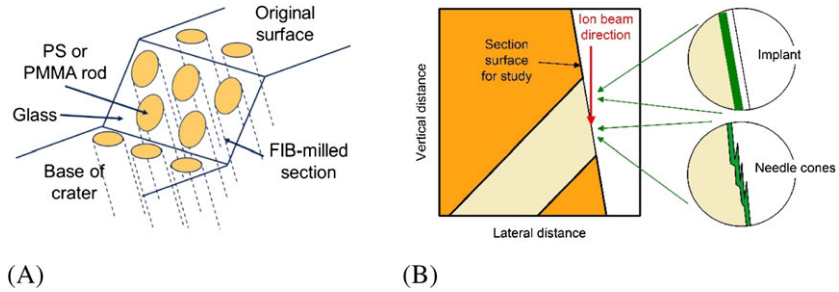

FIGURE 1 Schematic of polymer rods (light yellow) set in the glass structure (orangey-yellow in (B)) of the microchannel plate, A, showing the general arrangement of the focused ion beam-milled section and B, showing enlarged schematics with either an implanted layer (upper circle) or the needle cone structures (lower circle). In (B), the section is rotated 45° clockwise so that the Ga^+ ion beam direction is shown vertical by the red arrow and the final exposed section surface is inclined at 80° to the horizontal

occurred many times, associated with the overlayer removal, so that the SRIM calculations below, while correct for small doses, need modification for high doses.

In practice, the FIB-sectioning may be associated with some roughening. Long wavelength roughening (the undulations associated with roughness measurements) is not a problem because that is equivalent to averaging the results for a flat surface over a small range of angles. However, the development of any needle cone structures, which allow the tucking of Ga atoms "under" the average surface to submicron depths, would require much more extensive "cleaning" by the Ar^+ GCIB. Figure 1B shows, schematically, these 2 possibilities. Needle cones have been shown in metals after deep sputtering when impurities are present.[23] They have never been observed in organic materials. However, accumulation of Ga atoms could possibly nucleate needle cones. The closer the FIB-milled surface is to the FIB direction, the narrower and more improbable such cones become. Here we have 5° to 10° grazing incidence requiring the cones to be submicron in width. We shall deduce if needle cones are relevant from the measured data.

Figure 2 shows a selection of SRIM[24] computations for the low-dose implantation of 30 keV Ga^+ ions into pure PS at angles of incidence from 0° to 80°. We see a profile that is well described by a Gaussian distribution whose centroid depth and standard deviation reduce as the angle of incidence rises. Knock-ons and displaced C and H atoms are also computed and occupy the region up to this distribution.

In FIB sectioning, as a result of the continuous sputtering and removal of material, Ga atoms and damage will already be implanted at the shallower depths, ie, to the left of the distribution. It is therefore reasonable that the effective damage and implant depth are somewhat less than the centroid depth of the distributions computed using SRIM. For the flat samples, in what follows, we need to allow for the small amount of material removed by Ga^+ sputtering. The thickness, d, of PS sputtered by the total Ga^+ dose is 0.27 nm per Ga^+ ion/nm^2 from the AFM measurements across knife edges. We then remove $0.5d$ from the SRIM-computed implantation depth. We use $0.5d$ because the profiles for the last few ions will reach the full depth and only the first ion profiles will have had the full distance d removed by sputtering. In most cases, for the flat samples at 45° incidence, the effect of d is small.

4 | RESULTS AND DISCUSSION

Many profiles of the Ga^+ implanted flat PS surfaces were recorded for Ga^+, $C_7H_7^+$, and other positive secondary ions for different conditions. Example profiles are shown in Figure 3 for an implanted dose of 85 Ga^+ ions/nm^2 into PS surfaces at 0°, 60°, and 80° incidence angles. The $C_7H_7^+$ secondary ions are indicative of relatively undamaged polymer.

Figure 3 provides the dose to remove the implanted and damaged layer. We may calculate the sputtering yield of pure PS, Y in nm^3, for this condition using the equation[21]

$$\frac{Y}{n} = \frac{B(E/An)^q}{1+(E/An)^{(q-1)}} \quad (1)$$

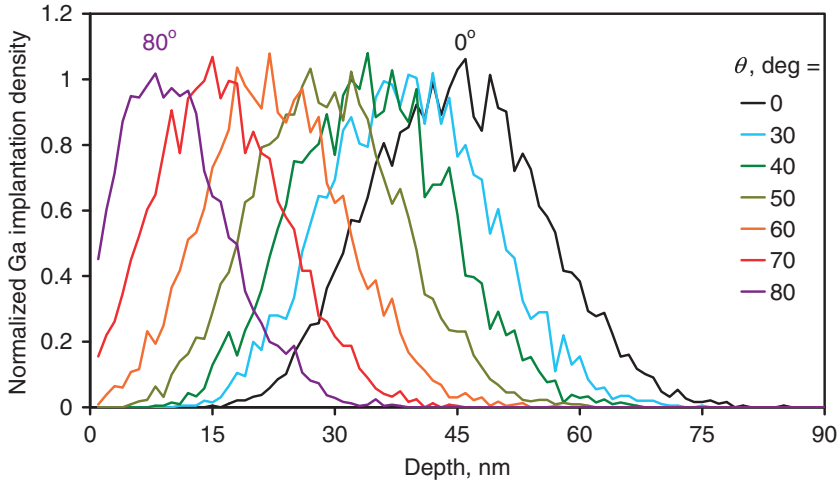

FIGURE 2 Stopping and Range of Ions in Matter computations for the implantation depth distributions, each for 5000 trajectories of 30 keV Ga^+ ions into pure poly(styrene) for many angles of incidence, θ

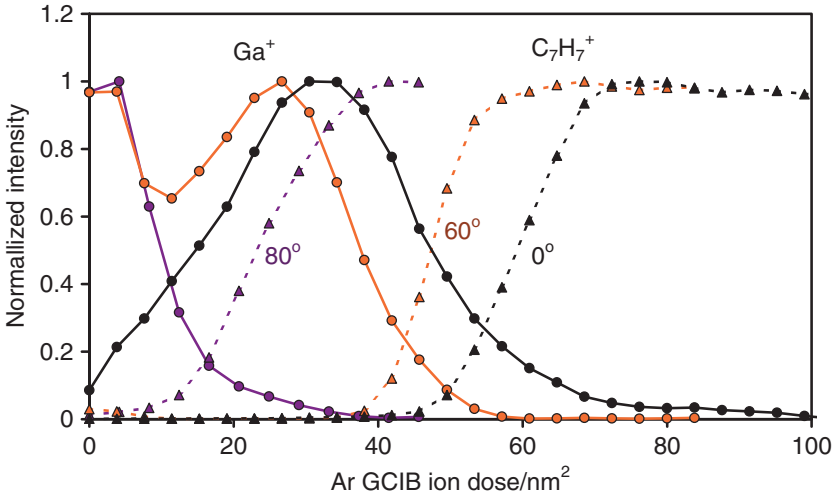

FIGURE 3 Measured depth profiles for Ga^+ and $C_7H_7^+$ secondary ions from samples of poly(styrene) implanted with 85 Ga^+ ions/nm^2 at 30 keV as a function of 10-keV Ar_{2500} cleaning dose at 45° incidence angle. The color scheme is the same as Figure 2 with black, orange, and purple for 0°, 60°, and 80° incidence angles, respectively. The solid lines joining circles are for Ga^+ and the dashed lines joining triangles for $C_7H_7^+$ ions

where E is the Ar^+ GCIB energy of 10 000 eV and n is the cluster size of 2500. For PS at 45°, the parameters A, B, and q are[21] 2.36 eV, 0.011 nm^3, and 3.4, respectively. Thus, Y = 37 nm^3. The dose to remove the Ga^+ and for the $C_7H_7^+$ signal to reach 50% for 60° implantation is about 60 Ar^+ GCIB ions/nm^2. This, combined with the sputtering yield of 37 nm^3, would appear to remove nearly 2 μm of pure PS rather than the 50 nm shown in Figure 2. For these flat surfaces, this high GCIB dose arises from the strongly reduced sputtering yield. It cannot be from the undercut of needle cones because the FIB doses implanted into the flat surfaces are at the wrong angle to generate the tilted needle cones required and are also insufficient to generate a needle cone structure.

The slow PS removal arises as the PS being removed is not pure; it is highly damaged and contains a high level of Ga atoms. Both of these effects reduce the sputtering yield. Our earlier analysis of both organic and inorganic materials[21] shows that at E/n = 4, the transition from organic to inorganic materials results in a reduction in sputtering rate of around 1000. The present situation indicates an interim position that we need to analyze more fully.

Figure 3 shows that, at a dose of nearly twice the centroid of the Ga^+ distribution, the $C_7H_7^+$ intensity has risen significantly in each case. We assume, first, that the sputtering rate is changed and is constant until the PS signal has risen to 50% because that gives the mean effective cleaning dose. For a pure PS spectrum, significantly more cleaning may be required, but the extent of that will depend on the depth resolution obtained. We cannot calculate the whole damage depth using SRIM, but the centroid of the Ga^+ implant depth may be calculated directly and may be compared with the centroid of the implant depth of the measured Ga^+ profile to give the effective Ar^+ GCIB sputtering rate during cleaning. The results of the SRIM computations are shown in Figure 4.

The data from Figures 3 and 4 give the measured and computed depths as Ar^+ GCIB dose and nanometers, respectively. From the centroids of the Ga^+ distributions, we may calculate directly the sputtering yield, Y^* in nm^3, for this damaged and Ga^+ implanted form of PS. In PS, the damage causes cross-linking, which will reduce the yield. Measurements by Cristaudo et al[25] show that the increase in molecular weight of PS with increased polymerization greatly reduces the sputtering yield. Seah[26] shows how this affects the parameter A in Equation (1). An increased bonding of only an extra C-C bond every 70 C atoms in low molecular weight material more than doubles the A value from 1 eV[26] to the fully polymerized value of 2.36 eV.[21] The presence of the Ga will also reduce the yield—eventually reducing it some 1000 times as we get to pure Ga where A would be ~50. Hence, we shall calculate Y^*/Y, and this may be expected to be in the range 0.001 to 1, depending on the damage and Ga content. We also need,

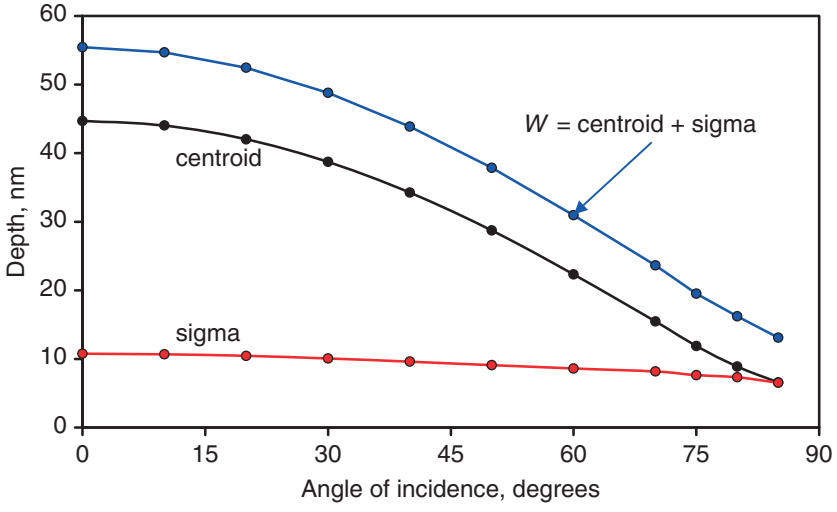

FIGURE 4 Depths for the Ga^+ parameters from Stopping and Range of Ions in Matter calculations at various angles of incidence in poly(styrene)

therefore, to calculate this effective Ga content, *G*. As shown in Figures 2 and 3, although all the implanted quantities there are 85 Ga^+ ions/nm^2, they are implanted to different depths such that the Ga density is much higher for studies at grazing incidence. At the different angles, the higher density and smaller depth partly counteract each other—one reducing the sputtering yield and the other reducing the amount of material to be removed. Assuming that the cross-linking and Ga effective depth, *W*, is the centroid depth of the Ga distribution plus 1 sigma, the Ga effective density, *G*, for Figure 3 is 85/*W* at/nm^3. *W* is shown in Figure 4.

To test the effect of the Ga^+ dose delivered, we have, on a different batch of PS, measured Ar^+ GCIB profiles for Ga^+ doses of 1, 5, 20, 40, 80, and 160 ions/nm^2 implanted at 45°. These show the total integrated Ga^+ SIMS signal to be proportional to this dose, and all exhibit very similar profiles, confirming these aspects of the above model. To match the SRIM calculations to the measured dose, we remove the 0.5*d* layer sputtered by the Ga^+ ions, where *d* (nm) = Ga^+ dose (ions/nm^2) × 0.27 (nm^3).

Figure 5 shows the result of the above computation as the 6 light purple circles. The highest implant levels show a more than 50-fold reduction in the sputtering yield compared with that for the pure material. To the left is a point at the low dose of 1.14 ions/nm^2 with only a 7-fold reduction. The ordinate, the fraction of the sputtering yield of the pure polymer, spans our sputtering rate range from 0.001 to 1. Through the PS data is a purple curve to guide the eye based upon Equation (1) with the effective bond-energy-related term *A* increasing with *G*. *A* starts at the value for pure PS of 2.34 eV at *G* = 0 and then increases with log (*G*) following an integrated exponential to a value near 10 eV at *G* = 5 at/nm^3.

Analysis of the data at different angles of incidence is more complex. We need the value of *d* for those angles. The angle dependence of this sputtering rate is calculated from the averages for PS and Ga using SRIM. This SRIM sputtering rate at 45° matches the 0.27 nm per Ga^+ ion/nm^2 measured at 45° by AFM. The amounts removed at 60° and 80° are significant, so much so that, at 80°, the implanted peak is lost. Repeated implantation may be considered as a series of implants and removals so that the experiment data are for the tail of this distribution which is calculated by summing many profiles, each more shifted by the sputtering loss, to have a centroid at 7.8 nm. This is matched to the measured dose for the centroid in Figure 5.

Added to Figure 5 are similar measurements extracted from Figure 4 of Iida et al's[27] detailed study for the Ar^+ GCIB cleaning of flat Ga^+ implanted, PC at 48° incidence. These are shown as orange circles and are for cleaning using 20-keV Ar_{2500}^+ at 40° incidence. For this condition, the sputtering yield of pure PC is 60 nm^3.[21,28] Iida et al[27] do not give the Ga^+ profiles but only the Ar^+ GCIB recovery dose as a function of the implanted Ga^+ dose. For our purposes, to determine the effective sputtering yield, we use the SRIM-calculated Ga^+ implantation depth in PC and a fraction of 57% of the recovery dose to allow for the difference between their measure of the recovery dose[29] and the centroid of the Ga^+ profile, assumed to be of a similar scaling to our data for PS. The remainder of the computation is as described above. The orange curve is to guide the eye in a similar manner to the purple curve, but the *A* value starts at the value of 4.2 eV for pure PC. Both curves asymptote to unity as *G* goes to zero.

The data so far have been for implanted flat surfaces where the total Ga^+ sputtering is insufficient to generate the needle cones or any significant roughness. The squared symbols in Figure 5 are from 3 FIB-milled sections of the hybrid glass and polymer samples shown in Figure 1. Note that the slope of the FIB-milled section means that these surfaces are not cleaned with the Ar^+ GCIB at 45° but with that beam at near normal incidence. At normal incidence, this sputtering yield is reduced by a factor ~1.8[30] compared with that at 45°. In Figure 5, the FIB-sectioned data are for PS (yellow and blue) and PMMA (pink-red) and are all computed for the Ar^+ GCIB normal to the local surface.[30] The effective Ga density is calculated from the total implanted dose, here 40 900 ions/nm^2, divided by the total depth

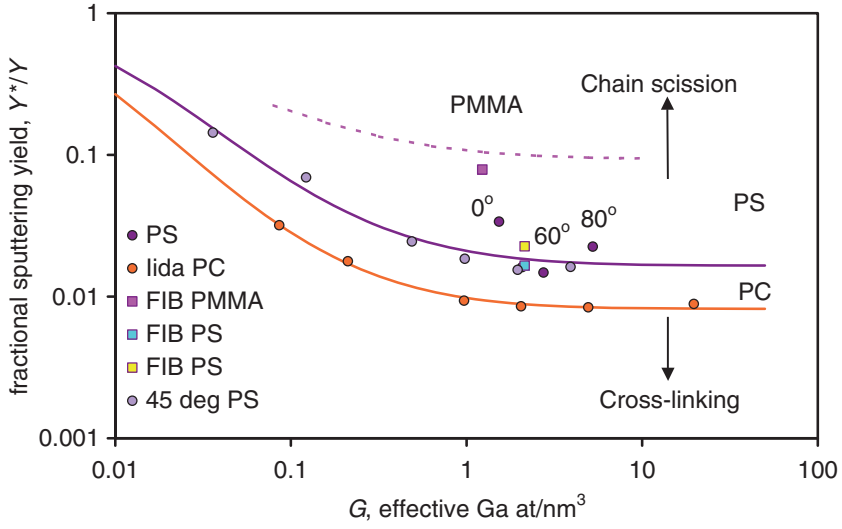

FIGURE 5 Plot of the fractional sputtering yields for each polymer versus the effective Ga density for various angles of incidence and operating conditions. Data given as circles are for implanting and cleaning on flat polymer surfaces, whereas the square symbols are for the cleaning of focused ion beam (FIB)-milled sections for poly(styrene) (PS). The light purple data are for PS surfaces implanted with 1 to 160 Ga^+ ions/nm^2 at 45° incidence; the darker purple data are at other angles of incidence. The yellow and blue squares are for FIB-milled sections of PS, whereas the pink-red square is for the FIB-milled section of poly(methyl methacrylate) (PMMA).[22] The orange data are from Iida et al's[27] detailed study for Ga^+ implantation in the surface of poly(carbonate) (PC). The solid lines are descriptions using Equation (1) with the parameter *A* increasing with *G* as described in the text. The dashed pink curve is the estimate for PMMA

of the cut, here 19 000-nm depth for PS and 33 000-nm depth for PMMA. The total depth of the cut can be measured directly from the SIMS images.[22] It may well be that these FIB Ga^+ contents have significant errors, although the depth predicted using SRIM starting at 45° and rising to 80° incidence is of a similar depth. However, the ordinate is insensitive to *G* in this region of Figure 5.

For the fractional sputtering yield, we need to determine the depth sputtered and the dose. The implant depth is calculated using SRIM[24] on the basis of no roughening with the final surface inclined at 10° to the Ga^+ FIB beam; ie, the Ga^+ angle of incidence is 80°. Because, in our FIB-milled section, we cannot use the Ga^+ signal, as that is dominated by signal from the FIB-milled glass area, we must use the signal for the PS recovery as shown in Figure 6. Figure 6 illustrates the recovery of PS signals for many ions with $100 < m/z < 150$. The Ga^+ and other signals that arise strongly from the FIB-milled glass surface are not shown. Cleaning the glass using the Ar^+ GCIB is significantly slower than the cleaning of the PS.[21] Using the scaling established for the flat samples, we reduce the dose for 50% recovery by a factor of 0.6 to give the centroid of the Ga^+ implant distribution to match the SRIM-calculated depth of this distribution. This generates the 3 square points in Figure 5. The agreement of the FIB-sectioned PS data with the flat sample data around 85 ions/nm^2 indicates that the low sputtering yield model applied to the flat samples also operates for the FIB sections. These data are consistent with an absence of needle cones in these FIB sections.

The effect of gallium bombardment on polymer chemistry has not been studied in detail, although specific systems have been addressed by Sezen et al.[31] The mechanisms would be expected to follow the general trends observed for other types of ionizing radiation.[32] Such radiation induces bond scission and the generation of both excited states and free radicals. The resulting effects depend upon their lifetimes, their mobility in the polymer, and the propensity to form low molecular weight, volatile products. Cross-linking generally occurs when 2 radicals on adjacent chains are close enough to form a bond. In all cases, both chain scission and cross-linking occur. Poly(styrene) is a well-studied polymer in this regard. It is able to form a long lived, stable benzylic radical without carbon-carbon bond scission. The radical has high mobility because of the numerous adjacent sites both within the chain and on neighboring chains. Poly(styrene) therefore tends to cross-link after exposure to radiation. It has been shown that the introduction of water vapor during Ga^+ ion bombardment of PS maintains a high sputtering rate, presumably due to the reaction of water with radical species and the prevention of cross-linking.[33]

Poly(methyl methacrylate) undergoes a number of reactions which result in the loss of volatile species and the scission of the main chain. Poly(carbonate) is also reported to predominantly undergo chain scission following irradiation,[32] although it is less clear that this is true under ion bombardment. Mahoney[34] classes PC as a type I cross-linking polymer along with PS, whereas PMMA is a type II degrading polymer involving random chain scission processes. In agreement with this, Cumpson et al[35] demonstrate that X-ray exposure during sputtering increases the sputtering rate of PMMA but not PS and PC. This latter study provides a direct comparison with PS and PMMA, showing the faster sputtering under combined X-ray and argon cluster beam sputtering than PS.

The study by Cristaudo et al[25] also shows how changing the bonding leads to a greater effect per bond in PS than PMMA. In the analysis of those data by Seah,[26] it is shown that the *A* value of PS changes 1.445 times more than that for PMMA for each added monomer. As the density of the end groups (no covalent bond to the next molecule) reduces, the *A* value increases. Equivalently, as the number of strong bonds increases, *A* will increase. If the above factor is used to convert the purple curve for PS to one for PMMA, by reducing the total change in *A* by this factor, we obtain the dashed pink curve that passes very close to the measured result for PMMA. This confirms the major effect of the adding or subtraction of bonds (ie, damage) in changing these sputtering rates.

The relative sputtering yield of Ga^+-irradiated PC in Figure 5 is shown to be lower than that of PS, which is not expected. This may be a result of the presence of gallium in the bombarded polymer changing the dominant mechanism of radiation damage. Gallium oxide, for example, has a highly exothermic enthalpy of formation (−1089 kJ mol^{-1}), and the removal of oxygen from the polymer could disturb the balance between chain scission and cross linking. We note that PS contains no oxygen and that gallium does not form stable carbide. The categorizations of Mahoney[34] and Cumpson et al[35] may thus be a rough first guide to the effects for many other polymers in Figure 5.

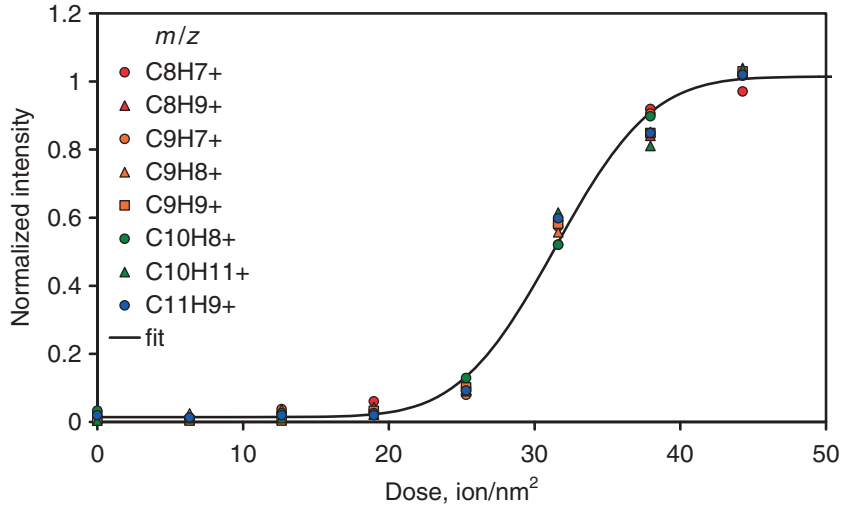

FIGURE 6 Depth profile showing poly(styrene) (PS) secondary ions from the sloping wall of the focused ion beam-milled hybrid PS-glass sample as a function of the 10-keV Ar_{2500}^+ ion dose. Note that the Ar^+ gas cluster ion beam is set nearly normal to the local surface. The profiles show the groups $C_xH_y^+$ with $8 \le x \le 11$ and $7 \le y \le 11$ as shown in the legend. The black line is a cumulative Gaussian fit with its mean at 31.5 ions/nm^2 and which gives the yellow square in Figure 5

Measurements involving implantation on polymer surfaces have been reported occasionally in the past. Miyayama et al,[18] studying polyimide, show, for a dose of 100 Ar^+ ions/nm^2, that the recovery dose using 10-keV Ar_{2500}^+ ions is ~13*E* ions/nm^2, where *E* is the energy of the implanted Ar^+ ions in keV. These are similar recovery doses to those shown in Figure 6, but, of course, there are no Ga atoms to remove. The easier removal of Ar may be offset by greater cross-linking in the polyimide. Similar measurements are reported by Yamamoto et al[36] for the damage caused by 1 ion/nm^2 of 10 keV normally incident Ar^+ implanted into PS. They find that there is a surface damaged layer of ~30 nm with a sputtering yield that is 0.23 of the value for undamaged PS. This damage thickness agrees with SRIM calculations of *W* and gives a result, in the counterpart of Figure 5 for Ar content, that is just above the purple line. It is likely that the implantation of Ga^+, rather than Ar^+ which may escape before analysis, accounts for this difference. Some very interesting data for 60-keV implantation of Bi_3^{++} into PS have been given recently by Kawashima et al.[37] At a Bi_3^{++} dose of 0.05 ions/nm^2 into PS, they show how the sputtering yield falls by a factor of 3 as the PS molecular weight reduces to 1200 Da. Low molecular weight material has a higher yield than fully polymerized PS.[25,26] The data for the highest molecular weight, when plotting versus Bi content, lie on the purple curve. These results for Ar^+ and Bi_3^{++} indicate that our analysis in Figure 5 may be applicable for all implanted species, not just Ga^+.

What Figure 5 shows very clearly is that the data from the smooth surfaces and the FIB-milled sections agree, indicating that the upper simple implant model of Figure 1B is appropriate and we do not need to consider the putative needle cones. It also shows that the cleaning requires a much greater dose than generally expected—but one that varies significantly with the organic material.

5 | CONCLUSIONS

We have shown that it is possible to remove the damaged and Ga^+-implanted layer remaining on polymeric materials when producing a FIB-milled section in a combined organic and inorganic structure. The sputtering rate for the damaged and Ga^+-implanted layer is about 55 times lower than for pure PS and 100 times lower for PC so that that layer behaves as though it were ~2 μm thick rather than 20 nm. The easier cleaning of the PMMA may arise from its lower propensity to cross-link. As indicated in Figure 5 and its associated analysis, it is expected that many implanted ions and organic layers will require this level of dose for effective cleaning. Those polymers that undergo bond scission during radiation will allow a faster removal of the damaged and implanted layer, whereas those undergoing cross-linking will require higher doses.

ACKNOWLEDGEMENTS

The authors would like to thank G McMahon for helpful discussions, I Mihara for helpful advice, and F Kollmer for the MCP used in making the reference sample. This work forms part of the 3D OrbiSIMS project of the National Measurement System of the UK Department for Business, Energy & Industrial Strategy. The work is further funded through the EMPIR Programme (Project "3DMetChemIT"). The EMPIR Programme is co-financed by the Participating States and from the European Union's Horizon 2020 Research and Innovation Programme.

CONFLICT OF INTEREST

The authors declare no competing financial interest.

ORCID

Mariavitalia Tiddia http://orcid.org/0000-0002-4634-1463
Martin P. Seah http://orcid.org/0000-0003-2633-3332
Alex G. Shard http://orcid.org/0000-0002-8931-5740
Guido Mula http://orcid.org/0000-0001-9364-6107
Rasmus Havelund http://orcid.org/0000-0001-7316-9761
Ian S. Gilmore http://orcid.org/0000-0002-0981-2318

REFERENCES

1. McMahon G, Nxumalo J, Phaneuf MW. Application of a novel FIB-SIMS instrument in SIMS image depth profiling. *Microsc Microanal*. 2002;8(suppl. 2):1212CD-1213CD.
2. McPhail DS, Chater RJ, Li L. Applications of focused ion beam SIMS in materials science. *Microchim Acta*. 2008;161(3-4):387-397.
3. Giannuzzi LA. Utlaut MA review of Ga^+ FIB/SIMS. *Surf Interface Anal*. 2011;43(1-2):475-478.
4. McPhail DS, Li L, Chater RJ, Yakoviev N, Seng H. From FIB-SIMS to SIMS-FIB. The prospects for a 10 nm lateral resolution SIMS instrument with full FIB functionality. *Surf Interface Anal*. 2011;43(1-2):479-483.
5. Li L, McPhail DS, Yakoviev N, Seng H. Strategies for improving the sensitivity of FIB-SIMS. *Surf Interface Anal*. 2011;43(1-2):495-497.
6. Whitby JA, Östlund F, Horvath P, et al. High spatial resolution time-of-flight secondary ion mass spectrometry for the masses: a novel orthogonal ToF-SIMS instrument with in situ AFM. *Adv Mater Sci Eng*. 2012. https://doi.org/10.1155/2012/180437, article number 180437, 13 pages;2012:1-13.
7. Schneider C, Weigand H, Rohnke M. Improving SIMS imaging of FIB bevel cuts with an elaborate sample holder. *J Vac Sci Technol B*. 2018;36(03):F101–1-F101–6.
8. Wilson RG, Stevie FA, Magee CW. *Secondary Ion Mass Spectrometry—A Practical Handbook for Depth Profiling and Bulk Impurity Analysis*. New York: Wiley; 1989.
9. Dowsett MG, Clark EE. Chapter 5 dynamic SIMS and its applications in microelectronics. In: Briggs D, Seah MP, eds. *Practical Surface Analysis, Volume 2: Ion and Neutral Spectroscopy*. Chichester: Wiley; 1992:229-301.
10. Briggs D. Chapter 7 static SIMS—surface analysis of organic materials. In: Briggs D, Seah MP, eds. *Practical Surface Analysis, Volume 2: Ion and Neutral Spectroscopy*. Chichester: Wiley; 1992:367-423.
11. Briggs D. Chapter 18 surface characterisation of polymers. In: Vickerman JC, Briggs D, eds. *ToF-SIMS Surface Analysis by Mass Spectrometry*. Chichester: Surface Spectra and I M Publications; 2001:497-524.
12. Leggett GJ, Vickerman JC. Effects of damage during the SIMS analysis of poly (vinyl chloride) and poly (methyl methacrylate). *Appl Surf Sci*. 1992;55(2-3):105-113.
13. Gilmore IS, Seah MP. Static SIMS: a study of damage using polymers. *Surf Interface Anal*. 1996;24(11):746-762.
14. Briggs D, Fletcher IW. Cs^+ ion beam damage of poly (vinyl chloride) and poly (methyl methacrylate) studied by high mass resolution ToF-SIMS. *Surf Interface Anal*. 1997;25(3):167-176.
15. Beamson G, Briggs D. *High Resolution XPS of Organic Polymers—The Scienta ESCA300 Database*. Chichester: Wiley; 1992.

16. Matsuo J, Toyoda N, Akizuki M, Yamada I. Sputtering of elemental metals by Ar cluster ions. *Nucl Instrum Methods B*. 1997;121(1-4):459-463.
17. Lee JLS, Ninomiya S, Matsuo J, Gilmore IS, Seah MP, Shard AG. Organic depth profiling of a nanostructured Delta layer reference material using large argon cluster ions. *Anal Chem*. 2010;82(1):98-105.
18. Miyayama T, Sanada N, Bryan SR, Hammond JS, Suzuki M. Removal of Ar^+ beam-induced damaged layers from polyimide surfaces with argon gas cluster ion beams. *Surf Interface Anal*. 2010;42(9):1453-1457.
19. Seah MP, Havelund R, Gilmore IS. SIMS of Delta layers in organic materials—amount of substance, secondary ion species, matrix effects and anomalous structures in argon gas cluster depth profiles. *J Phys Chem C*. 2016;120(46):26328-26335.
20. Havelund R, Seah MP, Gilmore IS. SIMS of organic materials—interface location in argon gas cluster depth profiles. *J Am Soc Mass Spectrom*. 2018;29(4):774-785.
21. Seah MP. Universal equation for argon gas cluster sputtering yields. *J Phys Chem C*. 2013;117(24):12622-12632.
22. Tiddia M, Mula G, Mihara I, Kollmer F, Seah MP, Gilmore IS, Havelund R. Chemical imaging of buried interfaces in hybrid organic-inorganic devices using FIB-TOF-SIMS, to be published.
23. Lewis GW, Kiriakides G, Carter G, Nobes MJ. Ion bombardment induced surface topography modification of clean and contaminated single crystal cu and Si. *Surf Interface Anal*. 1982;4(4):141-150.
24. Ziegler JF, Ziegler MD, Biersack JP. SRIM, the Stopping and Range of Ions in Matter, SRIM 2008–04, http://www.srim.org/.
25. Cristaudo V, Poleunis C, Czerwinski B, Delcorte A. Ar cluster sputtering of polymers: effects of cluster size and molecular weights. *Surf Interface Anal*. 2014;46(S1):79-82.
26. Seah MP. Argon cluster size-dependence of sputtering yields of polymers: molecular weights and the universal equation. *Surf Interface Anal*. 2015;47(1):169-172.
27. Iida S-I, Carr DM, Fisher GL, Miyayama T. Accurate and reproducible in-depth observation of organic-inorganic hybrid materials using FIB-TOF-SIMS. *J Vac Sci Technol B*. 2018;36(03):F107–1-F107–6.
28. Rading D, Moellers R, Cramer H-G, Niehuis E. Dual beam depth profiling of polymer materials: comparison of C_{60} and Ar cluster ion beams for sputtering. *Surf Interface Anal*. 2013;45(1):171-174.
29. Iida S-I. Cross-section observation of inorganic/organic materials by using FIB-TOF-SIMS. *J Surf Anal*. 2016;23(1):11-18.
30. Seah MP, Spencer SJS, Shard AG. Angle dependence of argon gas cluster sputtering yields for organic materials. *J Phys Chem B*. 2015;119(7):3297-3303.
31. Sezen M, Plank H, Fisslthaler E, et al. An investigation on focused electron/ion beam induced degradation mechanisms of conjugated polymers. *Phys Chem Chem Phys*. 2011;13(45):20235-20240.
32. Ivanov VS. *Radiation Chemistry of Polymers*. Utrecht: VSP; 1992.
33. Kochumalayil J, Meiser A, Soldera F, Possart W. Focused ion beam irradiation: morphological and chemical evolution in epoxy polymers. *Surf Interface Anal*. 2009;41(12-13):931-940.
34. Mahoney CM. Cluster secondary ion mass spectrometry of polymers and related materials. *Mass Spectrom Rev*. 2010;29:247-293.
35. Cumpson PJ, Portoles JF, Sano N, Barlow AJ. X-ray enhanced sputter rates in argon cluster ion sputter-depth profiling of polymers. *J Vac Sci Technol B*. 2013;31:021208–1-021208–11.
36. Yamamoto Y, Ichiki K, Seki T, Aoki T, Matsuo J. Ion-induced damage evaluation with Ar cluster ion beams. *Surf Interface Anal*. 2013;45(1):167-170.
37. Kawashima T, Morita H, Fukumoto N, Kurosawa T, Aoyagi S. Examination of ion beam induced damage on polymer surface using Ar clusters. *Surf Interface Anal*. 2016;48(11):1175-1180.

How to cite this article: Tiddia M, Seah MP, Shard AG, Mula G, Havelund R, Gilmore IS. Argon cluster cleaning of Ga^+ FIB-milled sections of organic and hybrid materials. *Surf Interface Anal*. 2018;1–8. https://doi.org/10.1002/sia.6522